



## Magnetic hysteresis parameters and Day plot analysis to characterize diagenetic alteration in gas hydrate-bearing sediments

Randolph J. Enkin,<sup>1</sup> Judith Baker,<sup>1</sup> Danis Nourgaliev,<sup>2</sup> Pavel Iassonov,<sup>2</sup> and Tark S. Hamilton<sup>3</sup>

Received 19 July 2006; revised 15 March 2007; accepted 3 April 2007; published 29 June 2007.

[1] The J meter coercivity spectrometer is a machine capable of rapid and simple measurement of magnetic hysteresis, isothermal remanence acquisition and magnetic viscosity of rocks and sediments. The J meter was used to study a suite of samples collected from strata in the gas hydrate-bearing JAPEX/JNOC/GSC Mallik 5L-38 well (69.5°N, 134.6°W) in the Mackenzie Delta of the northwestern Canadian Arctic. The Day plot of magnetic hysteresis ratios for these samples is exotic in that the points do not plot along a hyperbola as is usually observed. Rather, they plot as a scatter which is shown to contour into vertical slices using coercivity field ( $H_C$ ) or saturation magnetization ( $J_S$ ), and horizontal slices using the relative quantity of superparamagnetism ( $J_{SPM}/J_S$ ). Optical microscopy reveals that the magnetic minerals are detrital magnetite and authigenic greigite. Greigite is dominant in sands which in situ had >70% gas hydrate saturation and in silts in which gas hydrate growth was blocked by insufficient porosity. We infer that the silts were the accumulation sites for solutes which had been excluded from the pore waters in neighboring coarser-grained sediments during the course of gas hydrate formation. Consequently, we conclude that magnetic properties are related to gas hydrate-related processes, and as such, may have potential as a method of remote sensing for gas hydrate deposits.

**Citation:** Enkin, R. J., J. Baker, D. Nourgaliev, P. Iassonov, and T. S. Hamilton (2007), Magnetic hysteresis parameters and Day plot analysis to characterize diagenetic alteration in gas hydrate-bearing sediments, *J. Geophys. Res.*, *112*, B06S90, doi:10.1029/2006JB004638.

### 1. Introduction

[2] Natural gas hydrates are remarkable water-ice crystal cages which accumulate in sediments and host immense quantities of methane [Kvenvolden, 1993]. Interest in gas hydrates is largely motivated by their potential to store or release greenhouse gases, and the prospect that they may become an economic source of “environmentally friendly” fuel. Research is required to determine the factors which control the global distribution of gas hydrates. They are stable in cold high-pressure environments typical of continental shelves (>300 m below sea level) or below continental permafrost (below 200 m depth); however, they are only found in places with sufficient methane supply and porosity [Hyndman and Davis, 1992].

[3] The redox potential in sedimentary environments is sensitive to the inorganic mineral-fluid buffers and biolog-

ically mediated interactions involving hydrocarbons and sulphates. Magnetic methods are particularly useful for delineating the history of these processes because iron-bearing minerals are easily transformed between various oxide and sulphide states when their redox environment changes [e.g., Berner, 1984; Passier *et al.*, 2001]. While magnetic minerals only constitute about 1% of typical sediments, they can be detected and characterized rapidly, leading to higher stratigraphic resolution than is often possible by optical or geochemical means. Furthermore, magnetic remote sensing methods hold the potential to provide a new prospecting tool, once gas hydrate control of the magnetic system is better understood and calibrated.

[4] In this study, we present data from samples collected from the JAPEX/JNOC/GSC Mallik 5L-38 well (69.5°N, 134.6°W). The Mallik site is a major gas hydrate field in the Mackenzie Delta of the northwestern Canadian Arctic [Osadetz *et al.*, 2005]. The main goal of the 2002 program was a production test of natural gas from hydrates, complemented by an extensive suite of regional geophysics, well logging and recovered core studies by a multidisciplinary science team of more than 265 scientists and engineers [Dallimore and Collett, 2005b]. Scientific results are summarized in Geological Survey of Canada Bulletin 585 [Dallimore and Collett, 2005a].

<sup>1</sup>Geological Survey of Canada-Pacific, Sidney, British Columbia, Canada.

<sup>2</sup>Department of Geology, Kazan State University, Kazan, Russia.

<sup>3</sup>Department of Chemistry and Geoscience, Camosun College, Victoria, British Columbia, Canada.

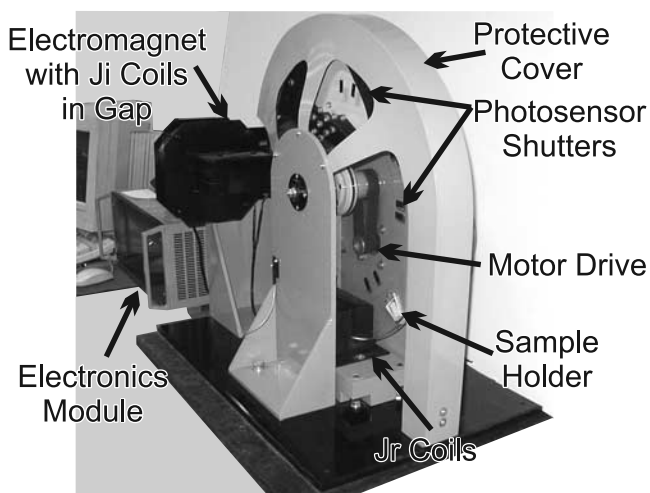


**Figure 1.** J meter coercivity spectrometer at the Geological Survey of Canada–Pacific paleomagnetism laboratory. The plastic disk (50 cm diameter, 1 cm thick) spins at 17.5 Hz, passing the sample through a magnetic field created by the electromagnet. During each rotation, the magnetic moment of the sample is measured within the field (induced magnetism, Ji channel) and in zero field (remanent magnetism, Jr channel). For each sample, the field ramps up from 0 to +500 mT and then down to –500 mT, followed by 100 s with 0 field.

[5] The interval from 885 to 1152 m depth was cored with 220 m of core recovered. *Medioli et al.* [2005] observed strong lithological control on gas hydrates concentration, especially the grain size and porosity. They occur mostly in the pore spaces in sand horizons, while silts host almost no hydrate. *Lowe et al.* [2005] presented the first magnetic results from this material, noting the strong contrasts in magnetic properties between the sands and silts. Magnetic susceptibility logging every 2 cm along the recovered core revealed that the silts have magnetic susceptibilities around 100–200  $\mu\text{SI}$ , an average of 2.7 times higher than that of the sands. This contrasts with the usual observation that sands hold similar or greater magnetic susceptibility than silts. Among the sands alone, there is a twofold decrease in magnetic susceptibility between strata with low and high gas hydrate concentrations.

[6] Paleomagnetic study of twelve subsamples suggested that the silts hold a primary remanence while the sands are remagnetized [*Lowe et al.*, 2005]. Acquisition of isothermal remanent magnetization measurements on this small collection led to the interpretation that the silts contain magnetite ( $\text{Fe}_3\text{O}_4$ ) while the sands which are magnetically weaker but harder contain an iron sulphide mineral (greigite?  $\text{Fe}_3\text{S}_4$ ). *Lowe et al.* [2005] suggested that processes correlated to the presence or flow of methane through the sand layers leads to the reduction of iron oxides to sulphides.

[7] An important implication of the findings is that magnetic methods may offer the potential for remote sensing of gas hydrates; however, very few samples were studied. In order to make feasible the study of magnetic properties of large numbers of samples, a new machine, the J meter coercivity spectrometer, was designed and built by

two of the authors (D. Nourgaliev and P. Iassonov). In this paper, we describe the theory and operation of this machine and present new results obtained from Mallik 5L-38 samples. The new magnetic measurements are complemented with optical microscopy on grain size separates and polished thin section observations, leading to an alternative interpretation for the observations than that reached by *Lowe et al.* [2005].

## 2. Methods

### 2.1. J Meter Coercivity Spectrometer

[8] The J meter coercivity spectrometer [*Burov et al.*, 1986; *Iassonov et al.*, 1998] is designed for studying ferromagnetic minerals contained in rocks and sediments by measuring magnetic hysteresis cycles and isothermal remanence magnetization (IRM) curves. Common practice is to measure hysteresis cycles with a vibrating sample magnetometer (VSM) (described by *Collinson* [1983, section 3.3.2]) in which a sample is oscillated within the pole pieces of an electromagnet, and secondary coils measure the sample magnetization. IRM acquisition curves are usually recorded by the method of stepwise magnetization, where remanent magnetization is impressed using an electromagnet and subsequently measured with a paleomagnetism magnetometer.

[9] The main element of the J meter is a pulse magnetometer, in which an electromotive force (EMF) pulse is induced in an array of pick-up coils by the magnetic field of a sample that moves at a high, constant speed past the coils. The sample is placed near the rim of a Plexiglas disk rotated at a constant speed by an electric motor (Figure 1). Pulse magnetometers are not used in paleomagnetic studies due to design drawbacks including the difficulty of screening of the sample from the external magnetic field, difficult reorientation of the sample, and a relatively high vibration level limiting the sensitivity of the instrument. However, the system is ideal for characterization of magnetic mineralogy. The combination of a pulse magnetometer and an electromagnet makes a simple (inexpensive) and robust system for the recording of magnetization curves. For this purpose, one of the sections of the sample's circular path is placed between the electromagnet poles to magnetize the sample. One set of pick-up coils are mounted directly on the pole pieces, similar to the geometry used for a vibrating sample magnetometer. The array is designed to present zero area turns to the applied field, so as to be sensitive only to the sample magnetization. The sample's within-field induced magnetization is measured as EMF pulses induced in this “Ji channel” set of coils. The magnetic remanence is measured with a second array of coils, called the “Jr channel”, situated away from the electromagnet and surrounded by a three-layer mu-metal shield (residual field below  $\sim 30$  nT). The spurious response generated by the instrument's vibration is attenuated by placing the Jr measuring coil and its shield on a heavy, damped platform.

[10] Both the induced and remanent magnetization are measured during each rotation of the disk. The electromagnet field is ramped slowly up to a set field (maximum 500 mT), and the down to the opposite polarity (–500 mT), making virtually continuous recordings of the hysteresis cycle with

the Ji channel, and the IRM acquisition and remagnetization curves with the Jr channel.

[11] For the present study, we use the J meter designed and built in 2005 for the Geological Survey of Canada laboratory in Sidney, British Columbia (Figure 1). Six previous J meters have been built and operated in Russia and Europe. The Plexiglas disk has a thickness of 1 cm and a diameter of 50 cm. It is rotated at 1050 rpm by an electromotor and is placed on a cushioned suspension to damp vibrations. The sample's position as it spins is monitored by a photosensor detecting light passed through the disk interrupted at places by opaque tape. The electromagnet's field intensity is measured the same way as the sample induced magnetism, but with a small electrically conducting copper ring placed on the disk opposite the sample. The diamagnetic field of Foucault currents in the ring induces EMF pulses in the Ji channel measuring coil that are proportional to the magnetic field intensity.

[12] The EMF pulses induced in the measuring coils are wavelets consisting of 3 peaks and valleys. The voltages are amplified, digitised and transmitted to a computer running a program in compiled Pascal that integrates the areas under the pulses. Calibration is calculated to first order from the geometry of the pickup coils, but it is refined by measuring a standard. The magnetic moment sensitivity of the Jr remanent magnetization measuring channel of the J meter is estimated at about  $5 \times 10^{-9}$  A m<sup>2</sup>, and the sensitivity of the Ji induced magnetization measuring channel at about  $5 \times 10^{-7}$  A m<sup>2</sup>. The duration of the experiment, consisting of recording about 4800 measurements of Ji and Jr as the field ramps from 0 to 500 mT and then down to -500 mT, followed by 100 s (1750 measurements) at zero field to measure viscous decay, is approximately 7 min. The rest field of the electromagnet after each hysteresis cycle is below 1 mT.

[13] The hysteresis loop and isothermal remanence acquisition curves of a moderately strong sample are illustrated in Figure 2. The standard hysteresis parameters can be derived from these graphs. The Ji channel records the sum of the hysteresis loop from ferromagnetic grains plus the paramagnetic or diamagnetic susceptibility of the rest of the sample (Figure 2a inset). Usually, the measured induced magnetization in fields stronger than 350 mT plots as a linear segment, the slope of which is the para(dia)magnetic susceptibility, recognizing that unsaturated ferromagnetic grains may tend to increase this value. After subtracting the high-field slope, the high-field extremes of the induced magnetism curve are horizontal at the value of the saturation magnetization,  $J_S$ . The remanence of saturation,  $J_{RS}$ , is the point at which the Ji curve crosses the  $H = 0$  axis. Because the Ji channel is noisier than the Jr channel, it is better to use the Jr channel to measure  $J_{RS}$ . After subtracting the induced magnetism of the paramagnetic component (Figure 2a), the coercive force ( $H_C$ ) is the backfield at which the induced magnetism is annulled ( $J_i = 0$ ). The coercivity of remanence,  $H_{CR}$ , is the backfield at which the remanence is annulled ( $J_r = 0$ ). Figure 3 presents results from a sample which is an order of magnitude weaker than that illustrated in Figure 2, and while the noise level appears quite large with the Ji channel, the coercivity parameters are still well defined.

[14] It is important to note that the hysteresis loop produced by the J meter is the sum of numerous minor loops, rather than a single hysteresis loop as is measured using a VSM. Despite the difference in methodology, the resulting curves should not be significantly different. As a test and an interlaboratory calibration, we measured 3 samples which were also measured using the Institute of Rock Magnetism (University of Minnesota) room temperature VSM (lab-modified Princeton Applied Research model PAR-155) (M. Jackson, personal communication, 2006). We have a sample of uncured Pozzolana cement containing oxidized pseudosingle-domain magnetite, and the two samples of crushed Tiva Canyon tuffs containing single-domain titanomagnetite, one with a large superparamagnetic population (announced in the *Institute of Rock Magnetism Quarterly*, issues 13(3), 2003; 14(3), 2004; and 16(1), 2006). The shapes of the curves measured on the two machines are nearly identical (Figure 4) other than a calibration difference of 9.5%. Since the main purpose of magnetic hysteresis work is to plot the differences between specimens within a study unit, the absolute calibration of the magnetometer is not critical. Variations in shape are minimal, with differences in the hysteresis parameter ratios  $J_{RS}/J_S$  less than 5% and  $H_{CR}/H_C$  less than 3%.

[15] In addition to the above parameters, the instrument provides a measure of the concentration of superparamagnetic grains in the samples (Figures 2b and 3b). When the field is reduced from its maximum value to zero, the remanent magnetization decreases due to the effect of thermal relaxation on the magnetization of magnetic grains with short relaxation times. The superparamagnetic magnetization ( $J_{SPM}$ ) is an informative parameter characterizing the concentration of superfine magnetic grains (<0.03  $\mu\text{m}$  for magnetite) with short relaxation times. The superparamagnetic grains are also measured during the 100 s viscous decay run which follows the hysteresis loop measurements (Figures 2c and 3c). The viscous decay follows a log(time) relationship [Dunlop, 1973], and the slope of this curve is roughly proportional to  $J_{SPM}$ . Perturbations to this curve can be used to probe the grain size distribution of the finest grains.

[16] The J meter is called a coercivity spectrometer because it is particularly well suited to measuring the IRM acquisition curve with sufficient sensitivity and resolution to take the derivative which defines the coercivity spectrum (Figures 2b and 3b). Typically, the spectrum can be well approximated by a lognormal curve; however, more advanced analysis can separate (or unmix) distinct populations of magnetic grains in each sample [e.g., Egli, 2003].

## 2.2. Samples

[17] Samples for the J meter were obtained by drilling the frozen core with an 8 mm drill bit and gathering 1.4 ml (1 to 2 g) of sediments in specially designed card boxes. The 198 horizons sampled were a representative set of the different lithologies and zones of different gas hydrate concentration. We particularly aimed at depth intervals with rapid changes in magnetic susceptibility.

[18] Gas hydrate concentration was measured using nuclear magnetic resonance well logs [Collett et al., 2005]. Well depths were converted to core depths using linear interpolation between a series of 21 wire line resistivity and

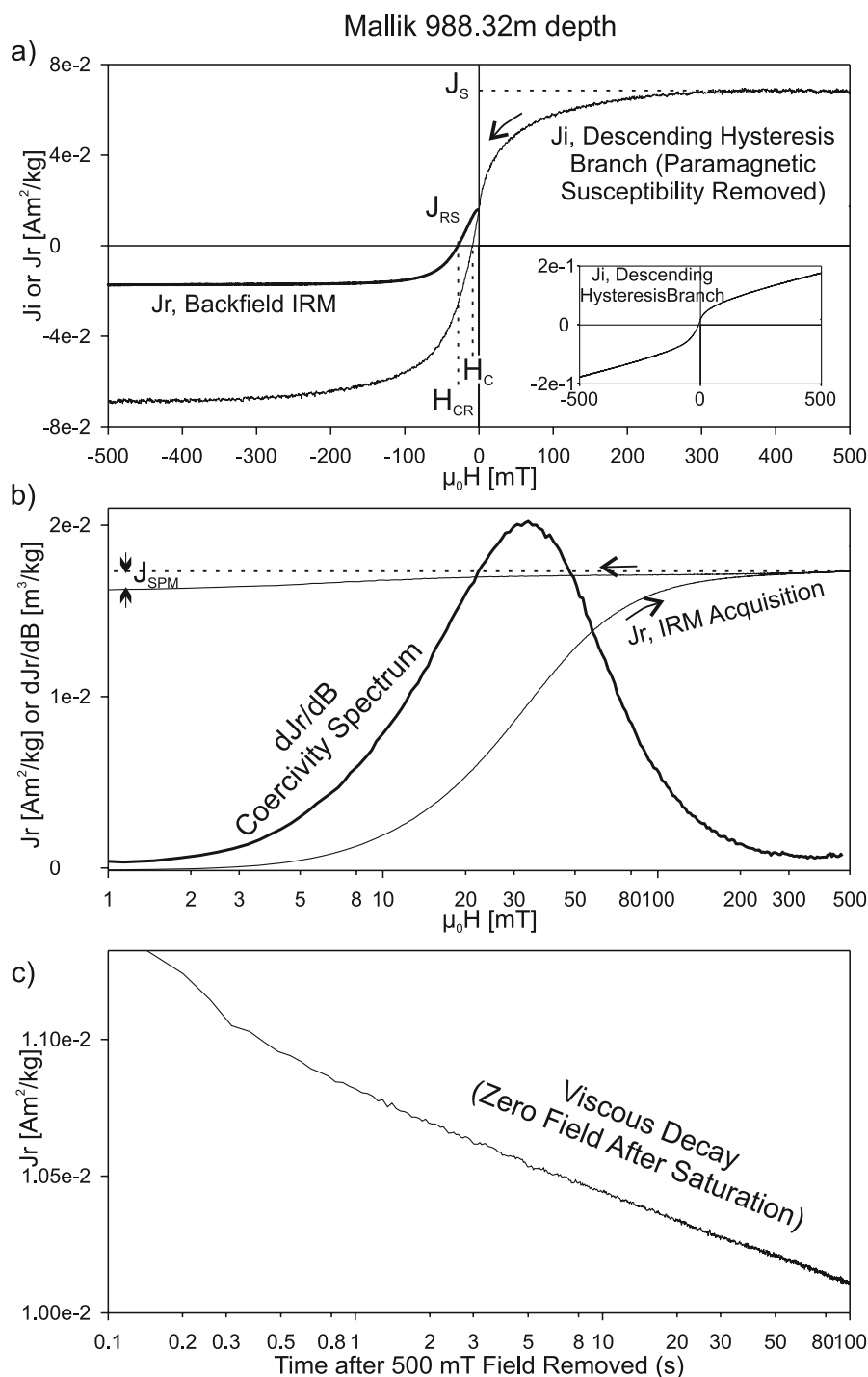


**Figure 2.** J meter results for a relatively strongly magnetic sample. Only raw data are presented, except for the  $dJ_r/dB$  coercivity spectrum in Figure 2b which is calculated after a running average smoothing of the  $J_r$  channel acquisition curve. (a) Descending hysteresis branch after saturation to 500 mT measured with the  $J_i$  channel. (The initial ascending branch from 0 to 500 mT is not shown.) The complete signal is presented in the inset, while the main diagram shows the hysteresis after paramagnetic susceptibility is removed. The bold line shows the backfield isothermal remanence (IRM) measured with the  $J_r$  channel (following the initial branch and the first half of the descending branch which are shown in Figure 2b). The hysteresis parameters saturation magnetization ( $J_s$ ), saturation remanence ( $J_{RS}$ ), coercive force ( $H_C$ ), and coercivity of remanence ( $H_{CR}$ ) are indicated. (b) IRM acquisition curve and its decay during removal of the field measured with the  $J_r$  channel. The superparamagnetic magnetization,  $J_{SPM}$ , is the measured decay in IRM between 500 mT and zero applied field, 2 min later. Bold indicates the derivative of the IRM acquisition curve, the coercivity spectrum. Note log scale for the field  $B = \mu_0 H$ . (c) Semilog time plot of viscous decay of remanence after removal of the -500 mT applied field.

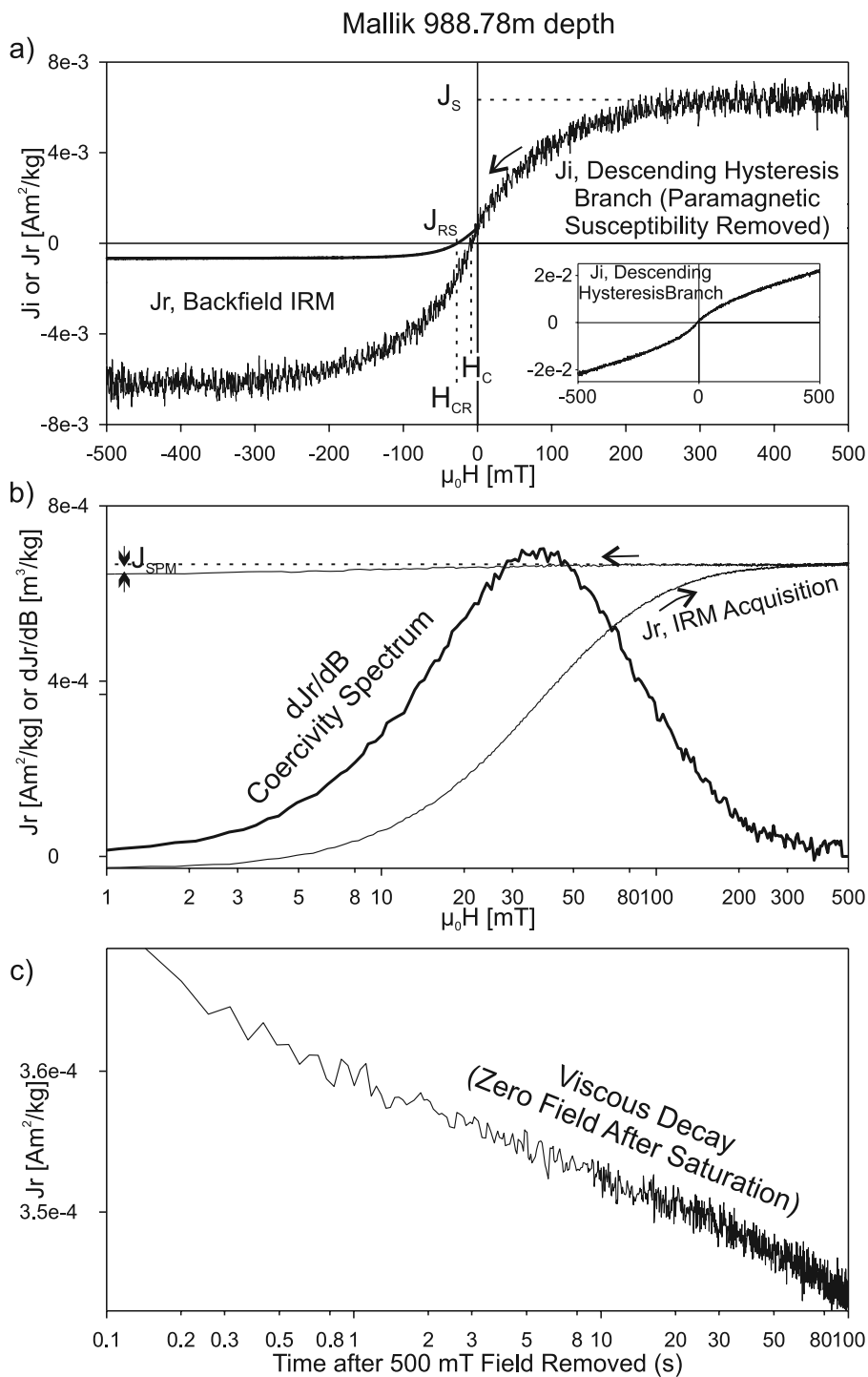


**Figure 3.** Same as Figure 2 except for  $J$  meter results for a relatively weakly magnetic sample. Despite the increased noise, all parameters remain precisely defined.

core log ties (S. R. Dallimore and P. Brennan-Alpert, unpublished data, 2004). Negative gas hydrate concentration estimates were set to zero and the data were linearly interpolated from their original  $\sim 16$  cm spacing to the depths of the magnetic samples.

[19] Figure 5 presents the core depths of the measured samples, along with the interpolated gas hydrate concentration, and the magnetic susceptibility ( $\chi_o$ , log scale) as

measured with a GF Instruments SM-20 hand-held susceptibility meter. The lithology, using the detailed logging reported by *Medioli et al.* [2005], is simplified to either silt (open triangles) or sands (solid squares). Most samples were collected from two gas hydrate zones, B (942–993 m) and C (1070–1107 m) [*Dallimore and Collett*, 2005b]. The well-logging measurements do not always have the depth resolution to show that the silts have lower gas hydrate

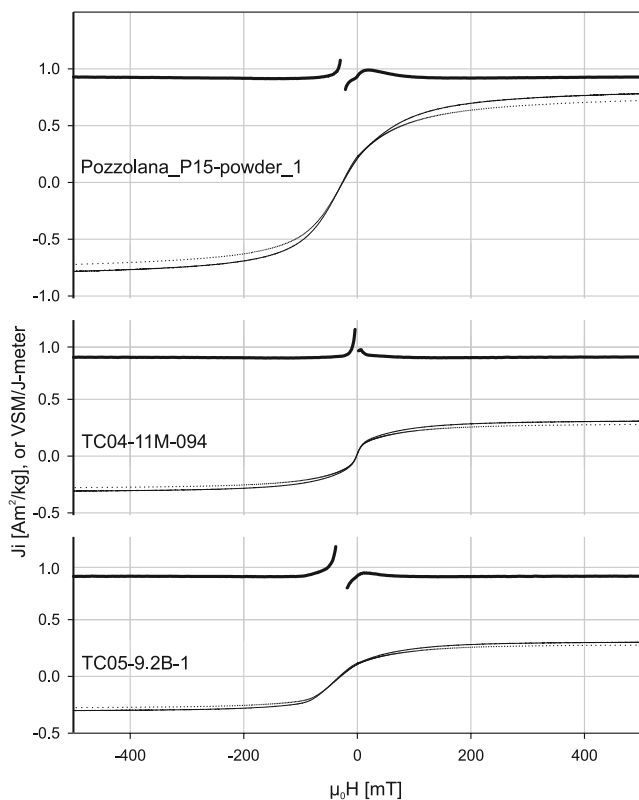


**Figure 4.** Interlaboratory comparison of three widely circulated samples (M. Jackson, personal communication, 2006). Only the descending paths from 500 mT to  $-500$  mT are illustrated. The dotted lines show results measured on a room temperature VSM (lab-modified Princeton Applied Research model PAR-155) at the Institute of Rock Magnetism, University of Minnesota. The solid lines are measured on the J meter at the Geological Survey of Canada–Pacific. The bold line is the ratio of the two measurements. Other than a 9.5% calibration difference, which was not corrected in order to show both curves, the two labs using apparatus with different mechanisms measured nearly identical hysteresis properties (maximum variation 7% except when the magnetization crosses zero).

concentration, but direct observations indicate that is the case.

### 3. Results

[20] Figure 5 also presents five parameters, measured with the coercivity spectrometer, which we find most useful

for analysis of these samples: the coercive force ( $H_C$ , linear scale), the coercivity ratio ( $H_{CR}/H_C$ , linear scale), the saturation magnetization ( $J_S$ , log scale), the magnetization ratio ( $J_{RS}/J_S$ , linear scale), and the ratio of superparamagnetism to saturation magnetization ( $J_{SPM}/J_S$ , log scale). While these parameters show noisy correlations to gas hydrate concentration and lithology, a few patterns do stand out. Samples with the lowest  $J_S$  and highest  $H_C$  values are all sands from the high gas hydrate zones (mostly between samples 130 and 160,  $\sim 1090$  m depth, but also between 20 and 45,  $\sim 970$  m depth). Other than these exceptional samples, silts (low gas hydrate content) tend to have lower  $J_S$  and higher  $H_C$  values than their neighboring sands (higher gas hydrate content). Silt samples have on average 2 times higher susceptibility than sand samples, and silts tend to have higher proportions of superparamagnetic grains, in keeping with their finer clast size.

[21] The “Day plot” ( $J_{RS}/J_S$  versus  $H_{CR}/H_C$ ) [Day *et al.*, 1977; Parry, 1982] is a useful way to discriminate between various magnetic mineralogies and grain sizes using coercivity and magnetization parameters. A Day plot of a collection of related samples often traces roughly along a mixing hyperbola, where  $(J_{RS}/J_S)(H_{CR}/H_C) = p$ , a constant on the order of 0.1 [Dunlop, 2002, equation (3)]. In contrast, the Day plot of the Mallik samples (Figure 6) is extraordinary in that the points do not follow any simple curve, but rather plot as a large scatter.

[22] We observe, however, coherent signals within the apparent scatter which are revealed by contouring the data. The contouring is done after Loess smoothing (locally weighted second-degree polynomial least squares fitting) to define a surface on a regular grid. When contoured by the coercivity,  $H_C$  (Figure 6a), the population resolves into roughly vertical ( $H_{CR}/H_C$ ) slices. Similarly, the population resolves into roughly vertical ( $H_{CR}/H_C$ ) slices when contoured by the saturation magnetization,  $J_S$  (Figure 6b). In this collection, there is apparently a monotonic relationship between  $H_C$  and  $J_S$ . Indeed,  $H_C$  is roughly proportional to  $J_S$  to the power  $-0.3$  (Figure 7).

[23] When the Day plot is contoured by the relative amount of superparamagnetism ( $J_{SPM}/J_S$ ), the data are sliced roughly horizontally ( $J_{RS}/J_S$ ). Thus the position on the Day plot is dependent on the proportion of the superparamagnetism and the value of saturation magnetization or coercive force. The apparent scatter is a function of two parameters. The J meter coercivity meter, having the capability of measuring the amount of superparamagnetism at the same time as the hysteresis parameters, is ideal for quantifying the effect. Other studies in progress in our laboratory reveal similar horizontal ( $J_{RS}/J_S$ ) slicing of the Day plot data when contoured by  $J_{SPM}/J_S$ , even though the data always fall

**Figure 5.** Results from samples collected from core recovered from the JAPEx/JNOC/GSC Mallik 5L-38 well. Squares indicate sands which tend to host gas hydrates, while triangles mark silts which are usually too impermeable to allow gas hydrate accumulation. The depth ranges of the principal gas hydrate zones are marked in the first graph. The gas hydrate concentration was measured using well logging nuclear magnetic resonance methods, and the depths were interpolated to core depths by matching features in the resistivity logs. Depths with intermediate gas hydrate concentration (50–70%) are highlighted with gray bands across the graphs. The magnetic susceptibility ( $\chi_0$ ) was measured with a hand-held susceptibility meter, while the following magnetic parameters were measured with the J meter: coercive force ( $H_C$ ), coercivity of remanence ( $H_{CR}$ ), saturation magnetization ( $J_S$ ), remanence of saturation ( $J_{RS}$ ), and superparamagnetic magnetization ( $J_{SPM}$ ).

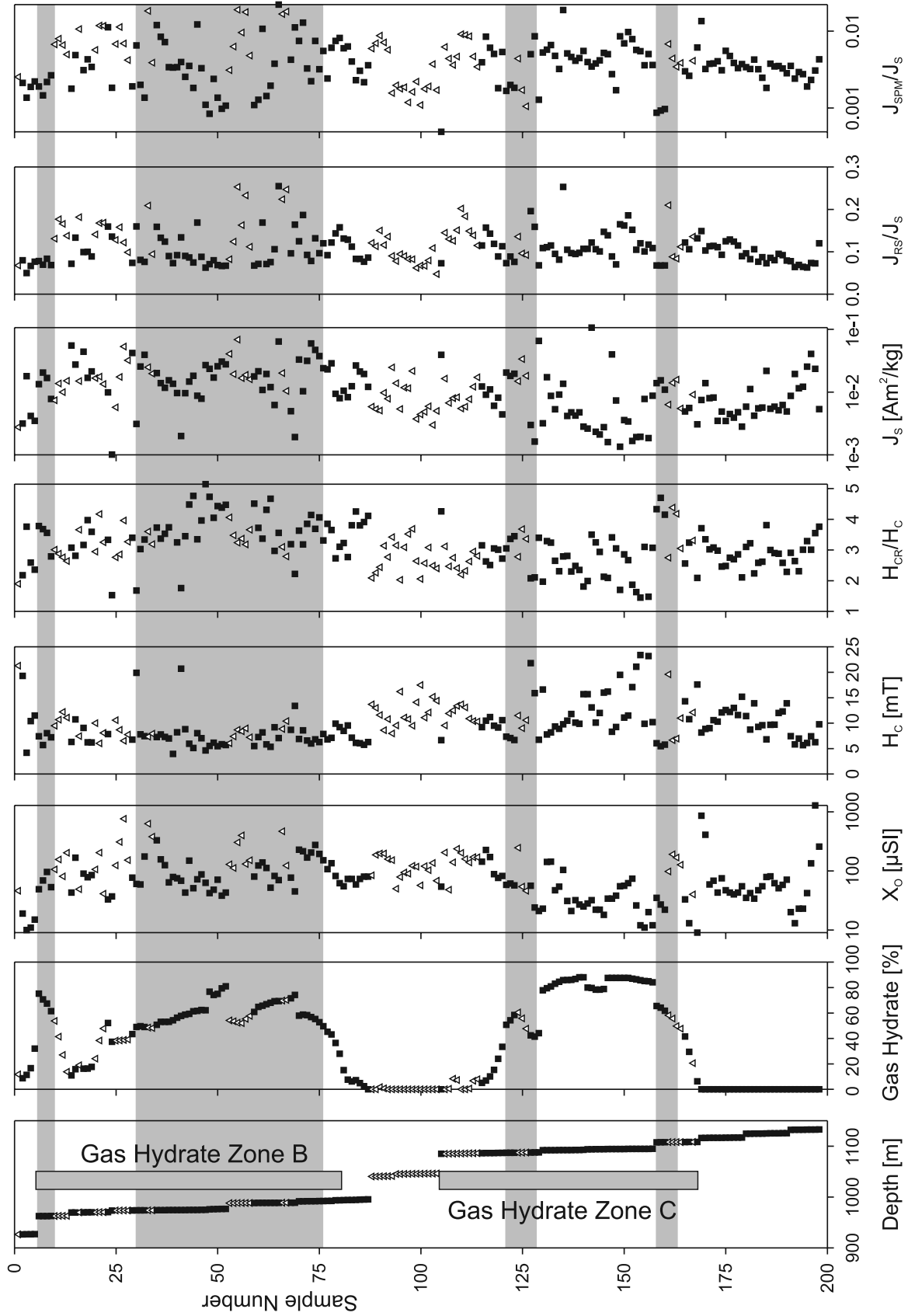
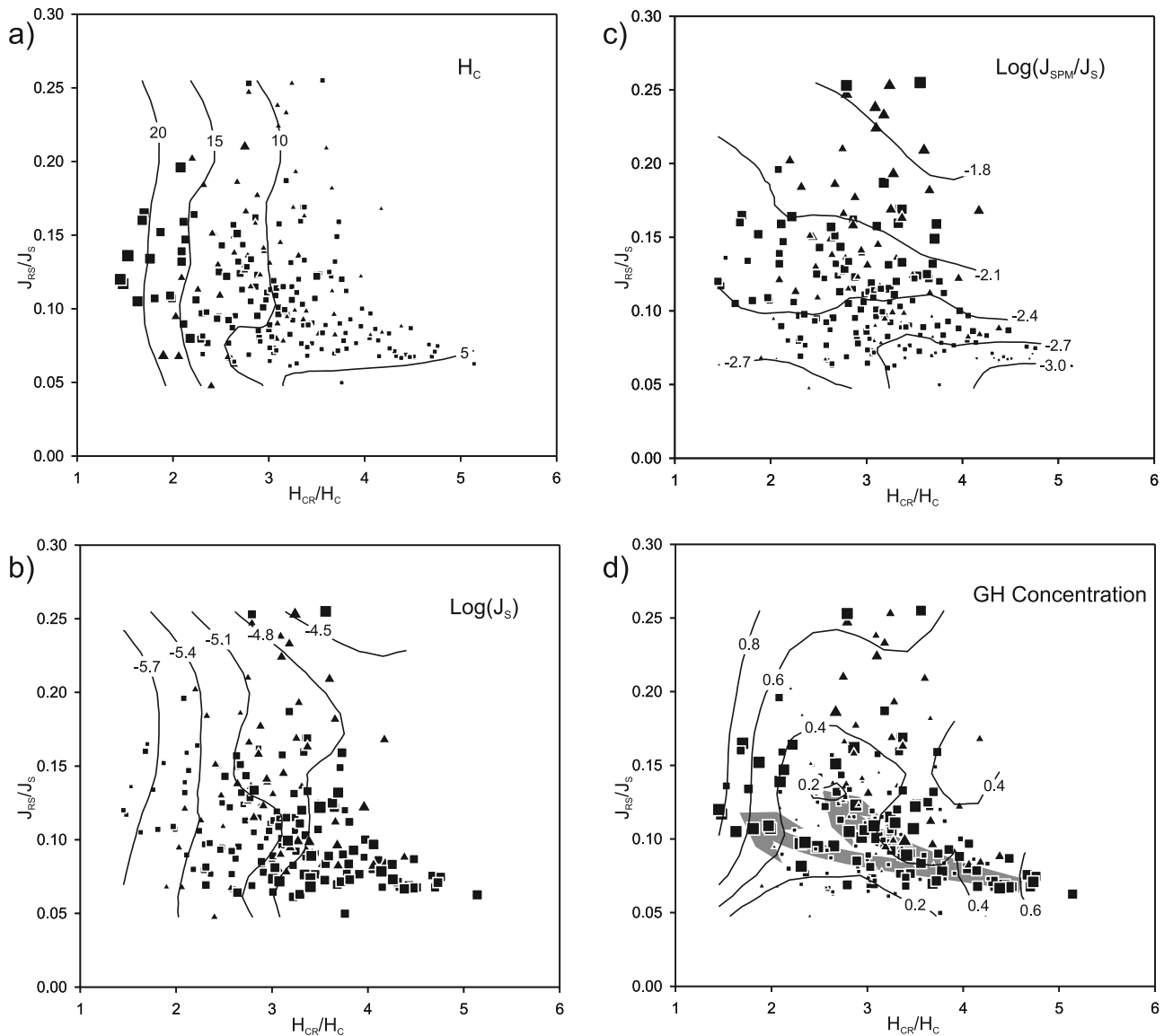


Figure 5



**Figure 6.** Day plots of hysteresis parameters. The data in each plot are identical, with squares marking sands and triangles marking silts. Only the symbol sizes vary, according to the parameter being contoured: (a) coercivity; (b) saturation magnetization; (c) relative quantity of superparamagnetism; (d) gas hydrate concentration. The contouring is done after Loess smoothing (locally weighted second-degree polynomial least squares fitting) to define a surface on a regular grid. In Figure 6d, the arrows show the proposed diagenetic pathways, from multidomain magnetite preserved in sediments which contain  $\sim 60\%$  gas hydrate to mixtures with more single-domain greigite either with higher or lower gas hydrate concentration.

closer to the familiar hyperbolic curve than those presented in this study.

[24] *Channell and McCabe* [1994] recognized that superparamagnetic grains make a sample plot up and to the right on a Day plot. *Tauxe et al.* [1996] simulated the effect numerically, and *Dunlop* [2002] modeled it theoretically. When our data are superposed on Dunlop's theoretical curves (Figure 8), we see that most samples fall around the mixing curve for single-domain and multidomain grains, with the high superparamagnetic samples approaching the curve for mixing single-domain and superparamagnetic grains. We observe that the effect of superparamagnetism

is different than predicted by Dunlop's model, because the contours of increasing superparamagnetism cut across the SD-MD mixing curves. More theoretical work is required to understand the interpretation on the Day plot in terms of grain size and domain state. Mixing curves for single-domain, multidomain and superparamagnetic grains all together must be constructed, rather than considering only two of these components at a time as has so far been modeled [*Dunlop*, 2002].

[25] On the basis of our preliminary study [*Lowe et al.*, 2005] we had expected to see a clear separation of magnetic properties with gas hydrate concentration. However,

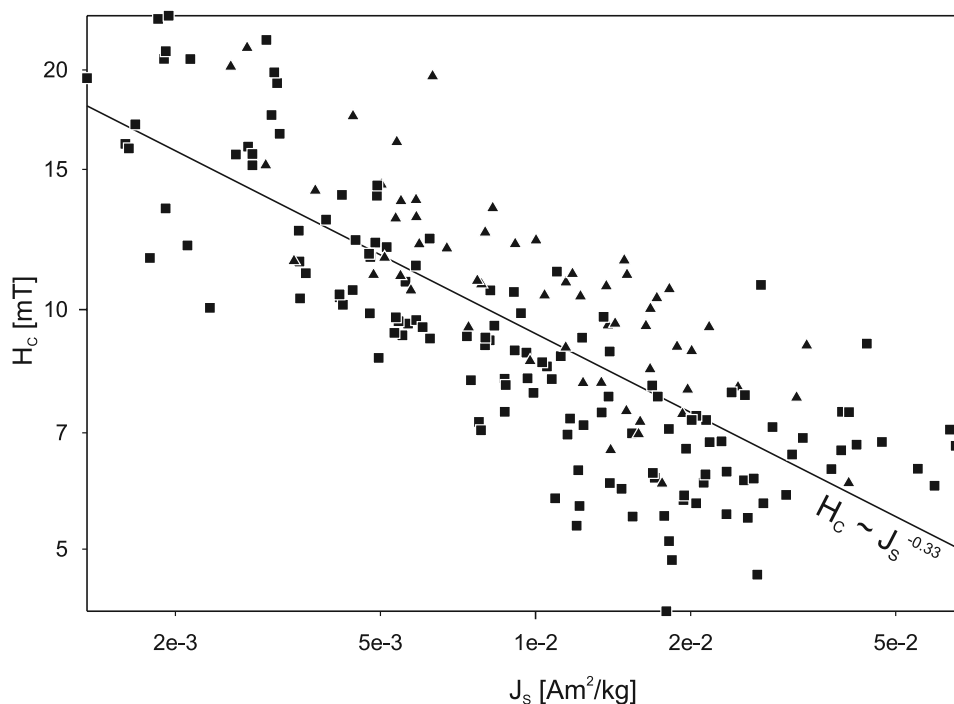


**Figure 7.** Coercivity versus saturation magnetization, showing a roughly monotonic relationship. The squares mark sand samples, and the triangles mark silt samples.

Figure 6d shows that the relationship is not as expected. Nevertheless, certain features are clearer on the Day Plot than when the hysteresis parameters are simply plotted by depth. We see a concentration of points with intermediate gas hydrate concentrations (50 to 70%) in the bottom right of the diagram, demonstrating domination by multidomain grains. Moving up and to the left on the Day plot indicates mixing single-domain or pseudosingle-domain grains with multidomain grains [Dunlop, 2002]. This appears to be the case for the samples with the lowest gas hydrate content (concentrated in the middle of the diagram) and the highest gas hydrate content (concentrated on the left side of the diagram). If only one magnetic mineral is present, then the different domain states reflect variations in grain size and shape. These effects can also be explained in terms of different magnetic mineralogy, since the grain size range for single-domain magnetic sulphides is much larger than for magnetite.

[26] Using  $H_{CR}/H_C$  as a proxy measurement for domain state, the dependence on gas hydrate concentration is clearer (Figure 9). The data are dispersed; however, the averages of  $H_{CR}/H_C$  calculated for each 10% wide window of gas hydrate concentrate forms a very smooth curve. As apparent on the Day plot (Figure 6d), the samples with the most multidomain magnetic behavior hold 50 to 70% gas hydrate concentration, and samples with more or less gas hydrate have more single-domain magnetic behavior.

#### 4. Petrography

[27] The diagenetic changes inferred from the magnetic measurements require complementary petrographic observations to identify the magnetic minerals and their origins. Twenty representative sediment samples were freeze dried

and impregnated with epoxy resin, to preserve the mineralogy and sedimentary texture, and prepared as polished thin sections for a reflected and transmitted light optical microscope study.

[28] The stratigraphy sampled had detrital magnetite as the most abundant primary magnetic mineral. Magnetite is often concentrated in a few thin laminae and is generally lower than a few percent by volume, especially in the unconsolidated sands. Detrital magnetites range in size from sand to silt grains in the clean quartz- and chert-rich, grain-supported, porous sands and sandy silts, to silt-sized grains in matrix-supported siltstones having a mud matrix and abundant authigenic cements (e.g., Figure 10a). Magnetites vary from apparently fresh, abraded cubic forms with bright gray reflectance and good polish to grains which are somewhat altered to leucoxene and hematite, showing reddish staining and taking a poorer polish. These appear to be inherited differences dependant on provenance of the original magnetite grains as both types can occur in the same section.

[29] The most abundant and ubiquitous magnetic mineral in the diagenetic assemblage is greigite, identified by its creamy white reflectance (unlike the brassy yellow reflectance of pyrite). This mineral is isotropic and tarnishes to a faint blue bireflectance (possibly secondary sulphide minerals like mackinawite) typical of tarnished greigite. Greigite is present in a variety of habits from 2  $\mu\text{m}$ -sized cubes and octahedra disseminated in the silt matrix to larger blades and framboidal masses (e.g., Figure 10b), up to veins and tubular masses of grains of a few mm across which are easily visible to the naked eye. These latter habits are the most striking as they are cross cutting with respect to depositional silt laminations and individual detrital grains,

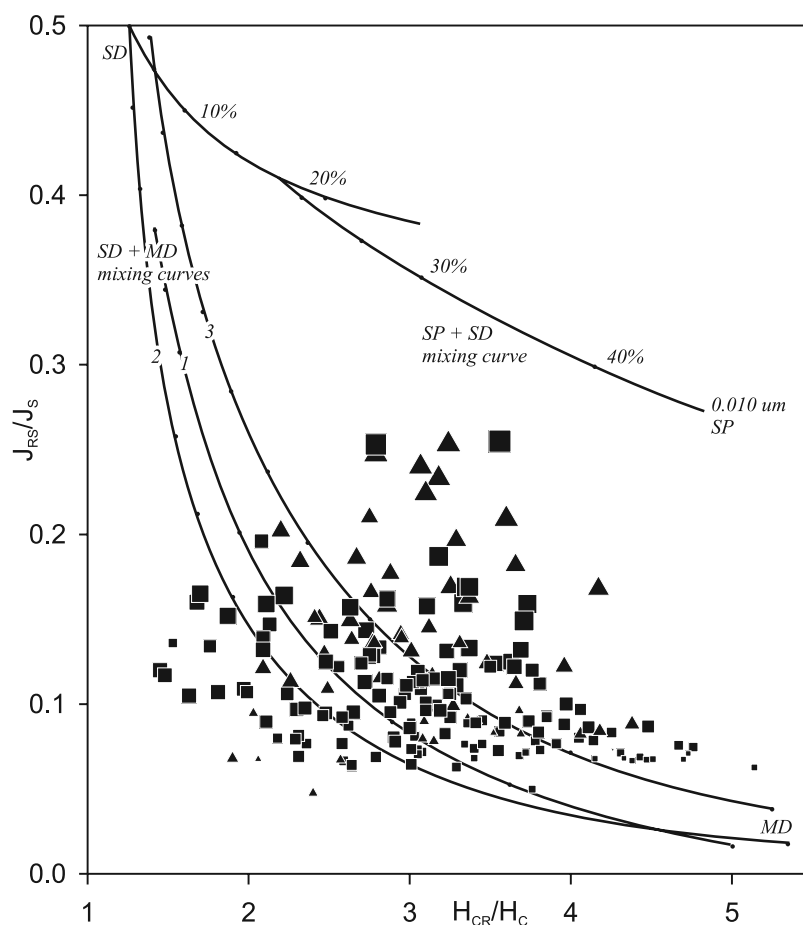


**Figure 8.** Same as Figure 6c superimposed on the mixing curves of Dunlop [2002] for single-domain (SD), multidomain (MD), and superparamagnetic (SP) grains.

especially in tensional veins and porphyroblasts which envelop other grains or inflate the structure of the sample. Greigite occurs in a diagenetic assemblage with radial and acicular clays, veinlets, layers and clots of inflationary carbonate cements (calcite, dolomite and siderite) and minor glauconite, jarosite, chlorite, azurite, malachite and pyrite. In most samples, but especially the silts, greigite is present in disseminated clots and patches throughout as fine idiomorphic grains. The distribution of greigite is somewhat laminar and often associated with stratified films of low-reflectance brown organic matter, as noted by Jenner *et al.* [1999].

[30] Greigite and magnetite are found in the same samples, often in different layers. The greigite porphyroblasts (poikiloblasts) sometimes envelope and totally overgrow detrital magnetite silt grains but entirely lack reaction textures at the contacts.

## 5. Interpretation

[31] The previous interpretation of reduction of iron oxides to sulphides in the presence of higher concentrations of gas hydrate [Lowe *et al.*, 2005] has to be reexamined in light of the present study. The main petrographic interpretation is that greigite formed preferentially in less permeable silty layers, which do not favor the growth of gas hydrate

[Clennell *et al.*, 1999]. The observation that greigite is concentrated in tensile veins and associated with fractured quartz grains in what are now unconsolidated sediments means that the diagenesis occurred when the sediments were frozen into a solid by hydrate cement. Furthermore, the low degree of organic maturation demonstrates that the sediments were never heated. The observed diagenetic textures are usually indicative of hydrothermal and skarn systems, dominated by rapid crystallization and introduced mineral phases. While in skarns and hydrothermal systems these textures are formed by boiling off pure water leaving a supersaturated residue, here the intense solute concentration mechanism is apparently achieved by the formation of gas hydrate freezing the sediment, and providing a solute-rich reactive solution outside the gas hydrate-bearing horizons [Jenner *et al.*, 1999].

[32] The lack of reaction of the detrital magnetite and the existence of both magnetite and greigite in the same layers argues against magnetite as the source of the iron for the formation of greigite. The greigites formed out of equilibrium, and in some places they, along with carbonates and clays, inflated the available pore space. New elements, including Fe, Ca, Mg, Mn, Cu and S, were introduced into sediments where they precipitated, perhaps quite rapidly as the observed assemblage of diagenetic minerals. The quartz

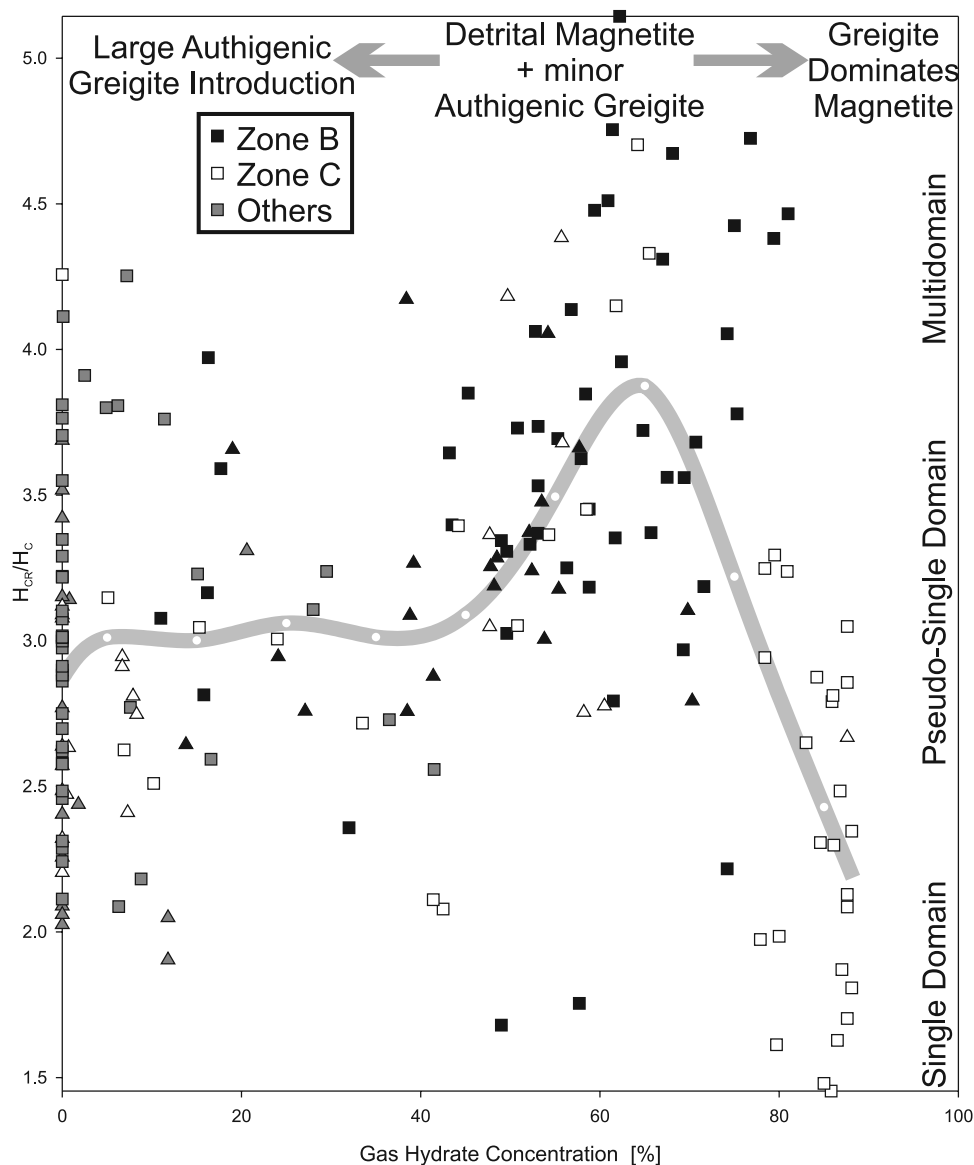


**Figure 9.** Relationship of the coercivity ratio, a proxy measurement for domain state, with gas hydrate concentration. The squares mark sand sample, and the triangles mark silt samples. The gray curve with the open circles is arithmetic means of  $H_{CR}/H_C$  values for each 10% slice of gas hydrate concentration. Between 50% and 70% gas hydrate concentration, the original detrital magnetite is inferred to dominate the magnetic behavior, since these samples in thin section appear to be the least diagenetically altered. At highest concentrations, the magnetite grains are interpreted to have been reduced to single-domain greigite leading to lower  $H_{CR}/H_C$  values. The samples with lowest gas hydrate concentration are the most affected by diagenesis, interpreted to be due to expulsion of solutes from the pore water during gas hydrate formation in neighboring coarser-grained sediments. The largest ranges of gas hydrate concentrations were observed in gas hydrate zone C near the bottom of the gas hydrate stability field, in which the full range of magnetic behavior (open symbols) was observed.

and chert dominated lithologies are an unlikely source for these elements. Possibly they are introduced along with the flux of methane-bearing fluids from depth. Irrespective of the source of these elements, the precipitation of greigite likely involved bacterially mediated sulphate reduction as a source of oxygen and methane as a source of food/fuel for the reaction. Within veins and also within pore throats, greigite often occurs as parallel swirls of microcrystals or

multinuclear colliform and framboidal masses suggesting the greigite formed on bacterial films. Coeval authigenic carbonates also appear to have been nucleated in pore spaces by bacterial processes [Medioli *et al.*, 2005].

[33] The formation of gas hydrate in the sands expelled the solutes from the pore waters into sediments ready to accept them. The silts and sands containing less gas hydrate were the main sinks for the brines; however, the magnetic

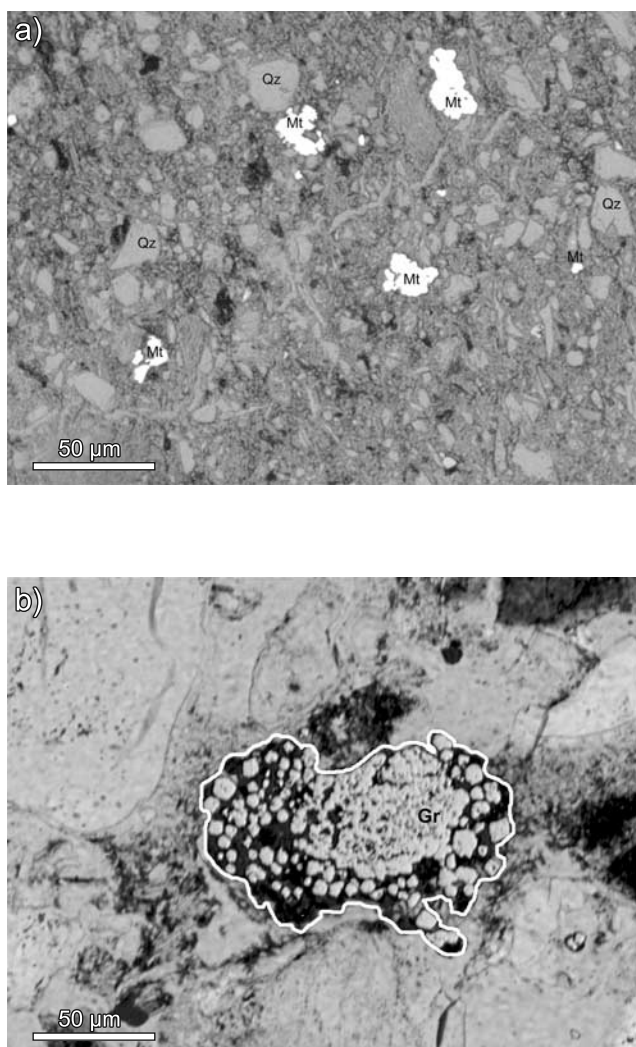


**Figure 10.** Photomicrographs of polished thin sections with both reflected and transmitted plane polarized light. (a) Horizon 1086.62m: matrix-supported sandy silt from laminated section of mixed silts and sands. Rounded detrital magnetite grains showing intense white reflectance are as large as quartz grains. Other sand and silt grains include lithic fragments and muscovite flakes. Note patch of scaly authigenic carbonate to left of largest magnetite grain. There is abundant fine grained carbonate cement of calcite and dolomite and curved en echelon veinlets of dolomite cutting this well-cemented siltstone. Magnetites are unreacted with respect to the introduced cements. (b) Horizon 1094.12 m: sand dominated by transparent quartz grains. White outline highlights and intergranular patch of authigenic cubes and framboids of creamy white reflectant greigite entirely filling a pore space between quartz, chert, and mica sand grains. Contrast the curved grain boundaries on the detrital sand to the delicate cubic geometries of the fine-grained introduced greigite cements.

transitions observed in the sediments almost saturated with gas hydrate suggest a similar process. In samples from 60 to 80% gas hydrate content, there is a significant change from multidomain to single-domain magnetic behavior (Figure 9). We consider that change, the accompanying decrease in

magnetic susceptibility, and the petrographic observation that opaques are scarce, requires dissolution of magnetite. Greigite is observed petrographically, and apparently dominates the remaining signal. The variations are argued to be diagenetic rather than due to source provenance differences, because the samples with the highest gas hydrate concentration in Zone C are bracketed by samples with ~60% gas hydrate concentration, presumably with similar source sedimentology, but which have multidomain characteristics (around samples 125, 1087 m depth, and 160, 1095 m depth, Figure 5).

[34] The thermal and methane flux history in these sediments may have been complex; however, we see petrographic evidence of a causal link between gas hydrate formation and sedimentary diagenesis, and a correlation between present gas hydrate concentration and the observed magnetic or petrographic properties. The implication is that each time gas hydrates accumulated in these sediments, the same diagenetic processes occurred. The sands have retained their porosity and methane flux pathways, while the silts, which did not allow gas hydrate formation, suffered a porosity decrease due to growth of authigenic minerals.

## 6. Conclusion

[35] The J meter coercivity spectrometer is an excellent tool for studying the magnetic properties of large suites of samples. It provides many useful magnetic parameters with rapid throughput. The simple design makes the machine more cost effective than other designs such as vibrating sample magnetometers.

[36] We illustrate the application of the tool on a study of unconsolidated sediments in a permafrost domain which hold a wide range of gas hydrate concentrations. The magnetic properties show a complex dependence on gas hydrate concentration. One analytical method which helps isolate the relevant magnetic properties is the Day plot of magnetic hysteresis ratios. The collection measured for this study does not follow a classic hyperbolic path on the Day plot, but thanks to analysis by David Dunlop, the apparently scattered distribution can be understood in terms of a mixing of multidomain, single-domain and superparamagnetic grains.

[37] A diagenetic pathway of iron minerals in this permafrost gas hydrate environment is proposed, in which original detrital magnetite remain unaffected and authigenic greigite is deposited. The latter forms as a result of bacterial activity with solute-rich pore waters (brines) which bring in Fe and S from elsewhere. The reaction is incomplete in most gas hydrate-rich horizons because the gas hydrate formation does not retain solutes. The horizons which least support gas hydrate formation are the most diagenetically altered, and the process happened rapidly when the sediments were largely frozen.

[38] Future magnetic measurements promise to refine our understanding of sediment diagenesis related to methane flux and gas hydrate formation. Bulk magnetic properties measured by the J meter coercivity spectrometer provide a rapid and cost-effective way of gathering magnetic data. This work potentially could lead to development of new proxy methods for gas hydrate studies.

[39] **Acknowledgments.** We thank the Mallik Consortium for providing the samples and Scott Dallimore for introducing us to the project. Ashley Dittmer assisted in the lab, and Lionel Esteban, Carmel Lowe, and Ted Irving commented on the manuscript. We appreciate the well-considered reviews of the journal's referees and Associate Editor, Alexei Smirnov. This work was supported by the Unconventional Gas Supply program of the Climate Change Technology and Innovation Initiative (Canadian Office of Energy Research and Development). The senior author had the privilege to have studied under David Dunlop, who we thank for providing insight and inspiration to the whole rock magnetism research community. This is GSC publication 20060732.

## References

- Berner, R. A. (1984), Sedimentary pyrite formation: An update, *Geochim. Cosmochim. Acta*, 48, 605–615.
- Burov, B. V., D. K. Nourgaliev, and P. G. Iassonov (1986), *Paleomagnetic Analysis* (in Russian), 167 pp., Kazan Univ. Press, Kazan, Russia.
- Channell, J. E. T., and C. McCabe (1994), Comparison of magnetic hysteresis parameters of unremagnetized and remagnetized limestones, *J. Geophys. Res.*, 99, 4613–4623.
- Clennell, M. B., M. Hovland, J. S. Booth, P. Henry, and W. J. Winters (1999), Formation of natural gas hydrates in marine sediments: 1. Conceptual model of gas hydrate growth conditioned by host sediment properties, *J. Geophys. Res.*, 104, 22,985–23,004.
- Collett, T. S., R. E. Lewis, and S. R. Dallimore (2005), JAPEX/JNOC/GSC et al. Mallik 5L-38 gas hydrate production research well downhole well-log and core montages, in *Scientific Results from the Mallik 2002 Gas Hydrate Production Research Well Program, Mackenzie Delta, Northwest Territories, Canada* [CD-ROM], edited by S. R. Dallimore and T. S. Collett, *Geol. Surv. Can. Bull.*, 585.
- Collinson, D. W. (1983), *Methods in Rock Magnetism and Paleomagnetism: Techniques and Instrumentation*, 517 pp., Chapman and Hall, New York.
- Dallimore, S. R., and T. S. Collett (Eds.) (2005a), Scientific Results from the Mallik 2002 Gas Hydrate Production Research Well Program, Mackenzie Delta, Northwest Territories, Canada, *Geol. Surv. Can. Bull.*, 585, 140 pp.
- Dallimore, S. R., and T. S. Collett (2005b), Summary and implications of the Mallik 2002 Gas Hydrate Production Research Well Program, in *Scientific Results from the Mallik 2002 Gas Hydrate Production Research Well Program, Mackenzie Delta, Northwest Territories, Canada* [CD-ROM], edited by S. R. Dallimore and T. S. Collett, *Geol. Surv. Can. Bull.*, 585.
- Day, R., M. Fuller, and V. A. Schmidt (1977), Hysteresis properties of titanomagnetites: Grain size and composition dependence, *Phys. Earth Planet. Inter.*, 13, 260–267.
- Dunlop, D. J. (1973), Theory of magnetic viscosity of lunar and terrestrial rocks, *Rev. Geophys.*, 11, 855–901.
- Dunlop, D. J. (2002), Theory and application of the Day plot ( $M_{rs}/M_s$  versus  $H_{cr}/H_c$ ) 1. Theoretical curves and tests using titanomagnetite data, *J. Geophys. Res.*, 107(B3), 2056, doi:10.1029/2001JB000486.
- Egli, R. (2003), Analysis of the field dependence of remanent magnetization curves, *J. Geophys. Res.*, 108(B2), 2081, doi:10.1029/2002JB002023.
- Hyndman, R. D., and E. E. Davis (1992), A mechanism for the formation of methane hydrate and seafloor bottom-simulating reflectors by vertical fluid expulsion, *J. Geophys. Res.*, 97, 7025–7041.
- Iassonov, P. G., D. K. Nourgaliev, B. V. Burov, and F. Heller (1998), A modernized coercivity spectrometer, *Geol. Carpathica*, 49, 224–226.
- Jenner, K. A., S. R. Dallimore, I. D. Clark, D. Pare, and B. E. Medioli (1999), Sedimentology of gas hydrate host strata from the JAPEX/JNOC/GSC Mallik 2L-38 gas hydrate research well, in *Scientific Results From JAPEX/JNOC/GSC Mallik 2L-38 Gas Hydrate Research Well, Mackenzie Delta, Northwest Territories, Canada*, edited by S. R. Dallimore, T. Uchida, and T. S. Collett, *Geol. Surv. Can. Bull.*, 544, 57–68.
- Kvenvolden, K. A. (1993), Gas hydrates-geological perspective and global change, *Rev. Geophys.*, 31, 173–187.
- Lowe, C., R. J. Enkin, J. Baker, and S. R. Dallimore (2005), Investigation of airborne magnetic data and magnetic properties of cored rocks from the Mallik gas hydrate field, in *Scientific Results from the Mallik 2002 Gas Hydrate Production Research Well Program, Mackenzie Delta, Northwest Territories, Canada* [CD-ROM], edited by S. R. Dallimore and T. S. Collett, *Geol. Surv. Can. Bull.*, 585.
- Medioli, B. E., N. Wilson, S. R. Dallimore, D. Paré, P. Brennan-Alpert, and H. Oda (2005), Sedimentology of the cored interval, JAPEX/JNOC/GSC et al. Mallik 5L-38 Gas Hydrate Production Well, Mackenzie Delta, Northwest Territories, in *Scientific Results from the Mallik 2002 Gas Hydrate Production Research Well Program, Mackenzie Delta, Northwest Territories, Canada* [CD-ROM], edited by S. R. Dallimore and T. S. Collett, *Geol. Surv. Can. Bull.*, 585.
- Osadetz, K. G., G. R. Morrell, J. Dixon, J. R. Dietrich, L. R. Snowdon, S. R. Dallimore, and J. A. Majorowicz (2005), Beaufort-Mackenzie Basin: A review of conventional and nonconventional (gas hydrate) petroleum reserves and undiscovered resources, in *Scientific Results from the Mallik 2002 Gas Hydrate Production Research Well Program, Mackenzie Delta, Northwest Territories, Canada* [CD-ROM], edited by S. R. Dallimore and T. S. Collett, *Geol. Surv. Can. Bull.*, 585.
- Parry, L. G. (1982), Magnetization of immobilized particle dispersions with two distinct particle sizes, *Phys. Earth Planet. Inter.*, 28, 230–241.
- Passier, H. F., G. J. deLange, and M. J. Dekkers (2001), Magnetic properties and geochemistry of the active oxidation front and the youngest sapropel in the eastern Mediterranean Sea, *Geophys. J. Int.*, 145, 604–614.
- Tauxe, L., T. A. T. Mullender, and T. Pick (1996), Pot-bellies, wasp-waists, and superparamagnetism in magnetic hysteresis, *J. Geophys. Res.*, 101, 571–583.

J. Baker and R. J. Enkin, Geological Survey of Canada, Pacific, PO Box 6000, Sidney, BC, Canada V8L 4B2. (renkin@nrcan.gc.ca)  
 T. S. Hamilton, Department of Chemistry and Geoscience, Camosun College, 3100 Foul Bay Road, Victoria, BC, Canada V8P 4J2.  
 P. Iassonov and D. Nourgaliev, Department of Geology, Kazan State University, Kremlyevskaya Str. 18, 420008 Kazan, Russia.